Letter Vol. 45, No. 6 / 15 March 2020 / Optics Letters 1301

Optics Letters

Producing anomalous uniform periodic nanostructures on Cr thin films by femtosecond laser irradiation in vacuum

Fei Wang,[1] Bo Zhao,[2,3] Yuhao Lei,[1] Jianjun Yang,[1,2,*] and Chunlei Guo[2]

[1]Institute of Modern Optics, Nankai University, Key Laboratory of Optical Information Science and Technology, Ministry of Education, Tianjin 300350, China
[2]State Key Laboratory of Applied Optics, Changchun Institute of Optics, Fine Mechanics and Physics, Chinese Academy of Sciences, Changchun 130033, China
[3]Department of Electronic Information and Physics, Changzhi University, Changzhi 046011, Shanxi, China
*Corresponding author: jjyang@ciomp.ac.cn

Received 7 November 2019; revised 10 January 2020; accepted 17 January 2020; posted 30 January 2020 (Doc. ID 382322); published 3 March 2020

We report on producing unprecedentedly uniform periodic structures on chromium thin films in vacuum conditions with irradiation of femtosecond laser pulses. In sharp contrast to the observations in air, the achieved surface structures of the ablated groove arrays are surprisingly found to have not only an extraordinarily uniform distribution but also a deep-subwavelength period of 360 nm. The measured both width and depth of the ablated periodic grooves are 150 and 120 nm, respectively, showing a large depth-to-width ratio and sharp-edge profiles. Remarkably, such well-organized nanostructures can be enabled to robustly extend into an infinitely long range via the sample scanning and even have a large-area production with a cylindrical lens. Raman spectral analyses reveal that the regular formation of such nanostructures benefits from avoiding the material oxidation and thermal disturbance of the air plasma on the sample surface.

https://doi.org/10.1364/OL.382322

Micro and nanoscale engineering of material surfaces has always been of great interest because of its capability in modifying the physicochemical properties of the sample interface, and it certainly expands the scope of material function for multidisciplinary applications [1–4]. To achieve this purpose, several top-down fabrication techniques, including photon/charged beam lithography and direct laser writing, have been established [5–8], which often however suffer high cost, low throughout, or long time consumption. Recently, femtosecond laser-induced surface structures, with a mask-free and single-step process, have attracted increasing attention by self-organizing the periodic patterns at subwavelength or nanometer scales [9–18], and this promises a powerful route for the high-speed laser processing beyond the diffraction limit.

For the strong absorbing metal materials, many previous reports proved that the femtosecond laser-induced structures typically exhibit orientation perpendicular to the direction of the light polarization, associated with a spatial period, Λ, slightly smaller than the incident laser wavelength ($\lambda > \Lambda > \lambda/2$) [10,11]. When the incident laser fluence is smaller, the onset of high-spatial-frequency surface structures can be achieved, whose spatial period becomes much less than the laser wavelength ($\Lambda < \lambda/2$) [16,17]. Nevertheless, the quality of such surface structures is usually observed to be very poor. For example, the surface morphology is not only varied or inconsistent with different parts of the laser-exposed surface area because of the Gaussian beam profile, but also possesses a quasi-periodic spacing with evident wavy, bending, or bifurcation. In particular, for the generation of the high-spatial-frequency structures, the structure arrangement is most likely to broken up into the short-range fragments, or the so-called structure period can only be measured within the nanoscale range. From an application prospect, methods to fabricate the uniform nanostructures within a long range are in fact a great challenge.

In this Letter, we demonstrate the fabrication of extraordinarily uniform structures on chromium (Cr) thin films, using the linearly polarized single-beam femtosecond laser pulses in vacuum condition. The well-organized structures appear to possess some striking features such as the anomalous uniform distribution, the deep-subwavelength period, and the ablated grooves with sharp edges and large depth-to-width aspect ratio. Remarkably, such nanostructures can be indefinitely extended into a large area through the sample translation, even with a cylindrically focused laser beam. Raman spectroscopic analyses reveal the important roles of the ambient air during the structure formation.

A schematic diagram of the experimental setup is shown in Fig. 1, where a chirped-pulse-amplification-based Ti:sapphire femtosecond laser system is used, which operates at a repetition rate of 1 kHz, with a time duration of 50 fs at the center wavelength of $\lambda = 800$ nm, and the output laser pulses are linearly polarized in the horizontal direction. After passing through attenuators, femtosecond laser pulses were guided into a vacuum chamber through a fused silica window onto a sample of

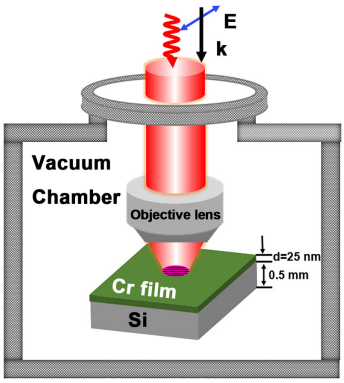

Fig. 1. Diagram of the optical path for femtosecond laser nanoprinting periodic structures on a thin Cr film placed in a vacuum chamber. **k** and **E** are the propagation vector and the polarization direction of the laser beam, respectively.

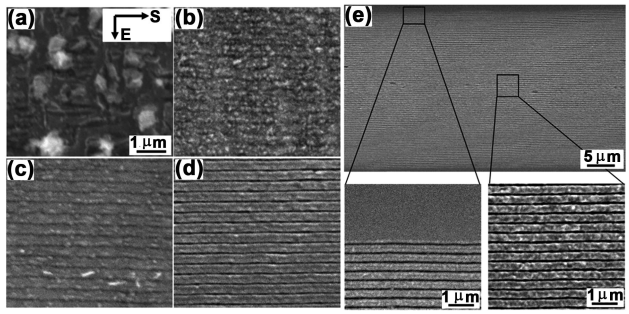

Fig. 2. Evolution of the surface morphology on Cr thin film induced by a femtosecond laser with air pressures in the chamber. (a) 1.0×10^5 Pa, (b) 1.0×10^4 Pa, (c) 1.0×10^3 Pa, (d) 5 Pa, and (e) 1.0×10^{-4} Pa. The energy fluence of the laser pulse is $F = 47.3\ \mathrm{mJ/cm^2}$. **E** and **S** represent directions of the laser polarization and the sample scanning, respectively.

25 nm thickness of Cr film (which is evaporated onto a single-crystal silicon substrate via a magnetron sputtering technique). An objective lens (4×, N.A = 0.1) was used to focus the laser at normal incidence, and the available beam spot diameter on the sample surface approximates 80 μm ($1/e^2$ intensity). During the experiments, the sample was moved perpendicular to the laser beam propagation with a slow speed of 2 μm/s, resulting in a number of near 40000 pulses partially overlapped within one spot area. The direction of the sample translation is perpendicular to the linear polarization of laser pulses. The morphology of the laser-exposed surfaces was characterized by scanning electron microscopy (SEM) and atomic force microscopy (AFM).

By adopting the laser energy fluence of $F = 47.3\ \mathrm{mJ/cm^2}$, we investigated how ambient air pressures in the chamber affect the surface morphology induced by femtosecond laser pulses, and the corresponding results are shown in Fig. 2. Clearly, for the cases of air pressure larger than of 10^4 Pa, we can only find random distribution of scratches or irregular-shaped bumps on the sample surface. When air pressure was reduced to 10^3 Pa, the periodic distribution of nanoscale lines began to develop on the laser-exposed surface, which is featured by the bulging profile and discontinuities. With the ambient air pressure continuously decreases down to 5 Pa, a clear appearance of d is presented on the surface, with the spatial orientation is perpendicular to the direction of the laser polarization. At first glance, this result is similar to the common observations on the surface of bulk materials that carried out in air circumstance reported in the previous studies[10,12]; however, the detailed inspection reveals that there are two unprecedented characteristics in our result: the measured spatial period of about $\Lambda = 360$ nm is less than the half of the laser wavelength, belonging to the deep-subwavelength regime, whereas the spatial alignment of the surface structures is highly regular without disintegrated irregularity such as wavy, bifurcation, and nanoholes.

As a matter of fact, it was found that the uniform periodic structures became more pronounced when the ambient air pressure in the chamber was lowered to as small as 1.0×10^{-4} Pa. As shown by the results in Fig. 2(e), under such vacuum condition, the formation of the surface structures clearly consists of a periodic array of the ablation grooves with a distinct and clean profile, especially in a relatively long spatial range. From the corresponding high-resolution SEM images, we can find that each ablation groove exhibits about 150 nm in width associated with the evidently sharp edges. In particular, by comparing the central and the periphery parts of the laser-exposed region, in which there are different intensity distributions for a Gaussian laser beam, the obtained periodic surface structures appear to have the identical profiles, which is in sharp contrast to the previous observations [13]. The fast Fourier transformation of the aforementioned structures is shown in Fig. 3(a), where a straight-line arrangement of the discrete tiny frequency spots indicates the high monotonicity of the structure period in the spatial domain. The inset picture shows the intensity profile curve of the straight-alignment frequency spots, wherein the identical interval between adjacent spots is measured as $f = 2.78\ \mu\mathrm{m}^{-1}$, and it indicates the corresponding reciprocal of the surface structure period. Remarkably, when the surface areas of the periodic surface structures were scanned once again by the femtosecond laser pulses at the same energy fluence, the homogenous distribution of the periodic ablation grooves can be well maintained rather than deteriorated during the sample translation, as shown in Fig. 3(b). Because the ablation grooves are spatially oriented parallel to the direction of the sample scanning, such uniform surface structures can be possibly extended in an infinitely long range without a discernible reduction in both the uniformity and distinct appearance. Moreover, we experimentally found that when the laser polarization was

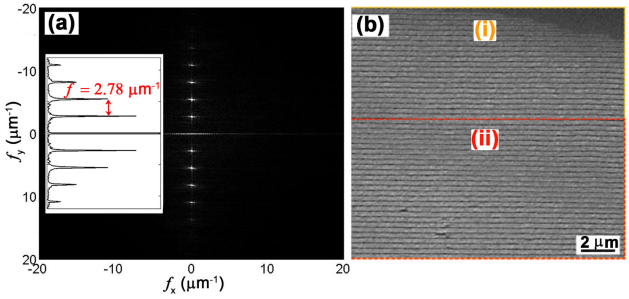

Fig. 3. (a) Image of the fast Fourier transformation for the periodic surface structures in Fig. 2(e), an inset picture for the intensity profile curve of the frequency spots. (b) Robustness of the periodic surface structures after twice scanning of femtosecond laser pulses, where (i) and (ii) regions stand for the structure formation by one and two times of the laser scanning, respectively.

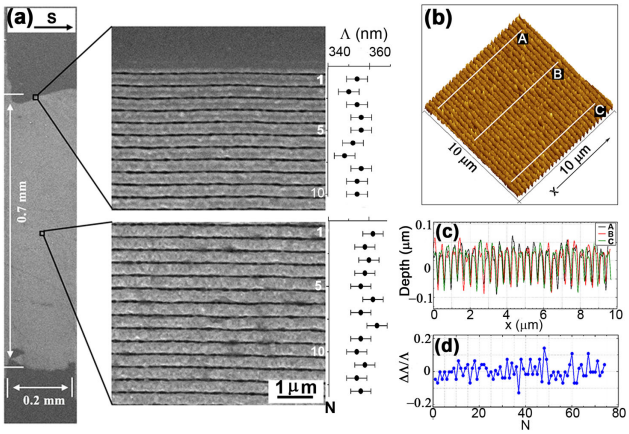

Fig. 4. (a) Obtained large-area uniform periodic surface structures on thin Cr film by focusing femtosecond laser pulses via a cylindrical lens under vacuum condition of 1.0×10^{-4} Pa. (b) AFM image of the periodic structures in Fig. 2(a). (c) Measured cross-sectional profiles of the surface structures. (d) Statistical fractional variations of the laser-induced structure period.

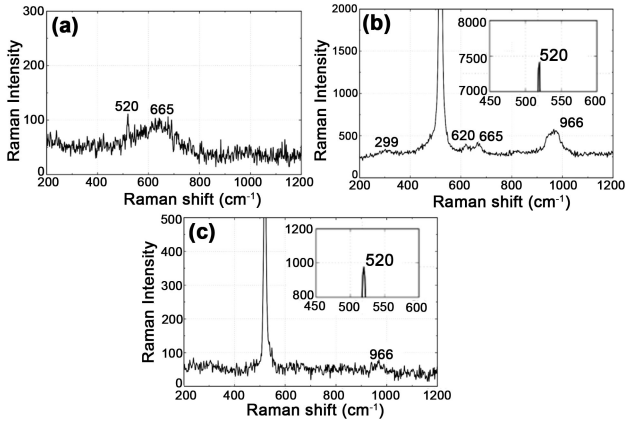

Fig. 5. Measured Raman spectra of the thin Cr/Si film under different experimental conditions: (a) without laser treatments, (b) at 1 atm air ambience, and (c) at the vacuum condition of 1.0×10^{-4} Pa.

parallel to the sample translation direction, the periodic surface structures also can be uniformly formed.

In order to improve the speed of laser nanofabrication, we replaced the objective lens by a fused silica-based cylindrical lens with a focal length of $f = 50$ mm, which can shrink the laser beam spot only in one dimension. When the air pressure in the chamber was kept at the vacuum condition of 1.0×10^{-4} Pa, a large area of uniform period surface structures was successfully achieved in one processing step, and the corresponding results are shown in Fig. 4(a). Under such circumstances, although the coverage width of the laser action area is as large as 0.7 mm, the ablated periodic subwavelength structure profiles appear to be almost the same, even at different positions, which is evidenced by the two zoom-in SEM pictures and the structure period measurements in the margin and center areas of the laser spot, as shown in Fig. 4(a). To quantitatively evaluate the uniform properties of the surface structure formation within a long range, we carried out AFM measurements for the topographical analyses, as shown in Fig. 4(b), in which three different sections (marked by the solid lines of A, B, and C) were selected for obtaining the cross-sectional profiles. From the topography curves in Fig. 4(c), we can gain some useful information as follows: (1) the spatial period of the surface structures is about $\Lambda = 360$ nm, which is consistent with that of SEM measurement; (2) within a 10 μm range, the structure period can keep almost invariant for each curve; (3) a good consistency occurs for the structure period of three different curves, which suggests that the generation of the periodic structures is physically locked during the sample scanning; (4) the measured ablation depth of the surface structures is approximately 120 nm; (v) the measured depth-to-width ratio of the structures is about $\gamma = 1$, which is much larger than that of the previous studies [18,19], which represents steep slopes of the ablated nanogrooves.

Moreover, by having statistics of the distances between adjacent dips in the above three curves (for a total number of 74 measured data), we obtain the fractional variations of the structure period over the large areas, and the statistical results are presented in Fig. 4(d). Clearly, most of the calculated values of $\Delta\Lambda/\Lambda$ are less than ± 0.1, which also indicates a high degree of spatial uniformity for the femtosecond laser-induced surface structures.

In addition, the material properties of the thin Cr film were characterized by Raman spectroscopy for trying to understand the mechanisms of the above phenomena, and the measurement results are shown in Fig. 5. Evidently, for the case of no laser treatment, the obtained Raman spectrum displays two weak peaks occurring at the positions of 520 and 665 cm^{-1}, respectively. The former is attributed to the silicon substrate indicating the optical penetration throughout the thin film [20]; the latter corresponds to the chromium oxide of CrO_2 [21], which suggests the existing slight oxidation before the laser irradiation. On the other hand, for the laser treatment under the air pressure of 1 atm, five distinct peaks began to appear in the Raman spectrum, with the positions at 299, 520, 620, 665, and 966 cm^{-1}, among which the strong peak intensity of 520 cm^{-1} indicates the great contribution from the silicon substrate. According to the refs [22,23], other four Raman peaks can be identified to the chromium oxides of Cr_2O_3 (299, 620 cm^{-1}), CrO_2 (665 cm^{-1}), and CrO_3 (966 cm^{-1}). This indicates that the oxidation of films becomes serious during the structure formation. More interestingly, when the film is treated by the laser pulses under the vacuum condition of 1.0×10^{-4} Pa, there are only two Raman peaks occurring in the measured spectrum, as shown in Fig. 5(c). Here one peak is at 520 cm^{-1} for the characteristic spectral line of silicon; the other peak takes place at 966 cm^{-1} with a relatively weak intensity, indicating the small amount of the chromium oxide of CrO_3 generated on the sample surface.

By comparing the above measurements of Raman spectra, we can recognize that the formation of highly uniform periodic surface structures is closely relevant to the depressed oxidization process of Cr films. Under the air pressure of 1 atm, the film oxidization is evidently pronounced to make the chemical change on the sample surface due to the laser heating with the substance of O_2. As a result, a certain amount of oxide material Cr_2O_3 is produced (whose intrinsic color of dark green is even observed on the surface by the naked eyes), and its higher melting temperature (2435°C) than that of Cr substance (1875°C) would like to improve the damage threshold of the sample surface, Moreover, the generation of oxide materials is ready to deteriorate behaviors of surface plasmon excitation at the given incident

laser fluence. Therefore, only some random distribution of the minor damages with a very shallow depth can be produced on the sample surface, rather than the formation of the periodic ablation traces. With reducing the ambient air pressure, the oxidization process of the film becomes weak, which makes the material surface predominated by the metallic substance of Cr. Under such a circumstance, the surface plasmon excitation becomes readily accessible, and its subsequent interference with the laser light can result in the intensity fringes and the spatially periodic ablation into the structures [10–12]. The lower the ambient air pressure, the weaker the oxidization process, and the depth of the periodic ablation on the sample surface becomes more prominent. Moreover, in contrast to the situations in air, for the laser irradiation under the vacuum conditions, there is no generation of the high-pressure air plasma prior to the ablation of material, which is caused by ionization of either a femtosecond laser pulse or the photoelectrons emitted from the sample surface, and usually remains acting on the sample surface for a time on the order of 10 ns [24]; that is, the thermal energy coupling on the sample surface will not be affected by both the laser energy stored in the air plasma and the heat in the restrained expansion of the material ejection, eventually leading to the decreased residual thermal energy deposition in the sample surface. Therefore, each surface region undergoing the ablation from the laser-plasmon interference is less disturbed by thermal instability of its surrounding areas, which accordingly leads to the highly localized formation of the nanogrooves with a clear profile and sharp edges.

In summary, we have investigated how the surface structures are produced on 25 nm thickness of Cr films irradiated by femtosecond laser pulses (1 kHz, 800 nm, and 50 fs) in the chamber with different air pressures. With the gradual decrease of the ambient air from the standard atmospheric pressure to 1.0×10^{-4} Pa, the appearance of surface structures has transitions from the random scratches followed by the periodic bulge-like nanolines to the extremely uniform array of ablated nanogrooves. In particular, the newly observed latter case can present some unique characteristics: the measured spatial period is shrunk into the deep-subwavelength scale of 360 nm and keeps almost unchanged on both the central and periphery areas of the laser exposure; each ablated groove associated with distinct and sharp edges tends to have the nanoscale width of 150 nm and depth of 120 nm, respectively; the unprecedentedly uniform distribution property can be robustly produced in a large range. To be frank, such striking features are nominally unachievable with the conventional techniques of femtosecond laser fabrication.

Raman measurements and analyses have suggested that the formation of surface structures is closely relevant to the involvement of air substance during the laser-material interaction, i.e., the oxidation process and the air plasma generation on the sample surface. The lower the ambient air pressure, the weaker the air involvement becomes, and the lesser disturbance from either the material chemical change or the air plasma assisted thermal energy transfer is obtained; thus, the structural regularity can be more improved. We believe that our investigations benefit the high-quality nanostructuring of a material surface and have potential applications in nanophotonics, plasmonics, and photon detection.

Funding. National Natural Science Foundation of China (91750205, 11674178); Jilin Provincial Science Technology Development Project (20180414019GH); Natural Science Foundation of Tianjin City (17JCZDJC37900); K.C.Wong Education Foundation (GJTD-2018-08).

Disclosures. The authors declare no conflicts of interest.

REFERENCES

1. M. E. Stewart, C. R. Anderton, L. B. Thompson, J. Maria, S. K. Gray, J. A. Rogers, and R. G. Nuzzo, Chem. Rev. **108**, 494 (2008).
2. A. Y. Vorobyev and C. Guo, Appl. Phys. Lett. **94**, 224102 (2009).
3. M. Liu, S. Wang, Z. Wei, Y. Song, and L. Jiang, Adv. Mater. **21**, 665 (2009).
4. J. J. Greffet, R. Carminati, K. Joulain, J. P. Mulet, S. Mainguy, and Y. Chen, Nature **416**, 61 (2002).
5. D. Winston, V. R. Manfrinato, S. M. Nicaise, L. L. Cheong, H. Duan, D. Ferranti, J. Marshman, S. McVey, L. Stern, J. Notte, and K. K. Berggren, Nano Lett. **11**, 4343 (2011).
6. H. Sai, Y. Kanamori, and H. Yugami, Appl. Phys. Lett. **82**, 1685 (2003).
7. M. Campbell, D. N. Sharp, M. T. Harrison, R. G. Denning, and A. J. Turberfield, Nature **404**, 53 (2000).
8. S. Juodkazis, V. Mizeikis, K. K. Seet, M. Miwa, and H. Misawa, Nanotechnology **16**, 846 (2005).
9. J. Reif, F. Costache, M. Henyk, and S. V. Pandelov, Appl. Surf. Sci. **197**, 891 (2002).
10. J. Wang and C. Guo, J. Appl. Phys. **100**, 023511 (2006).
11. Y. Tang, J. Yang, B. Zhao, M. Wang, and X. Zhu, Opt. Express **20**, 25826 (2012).
12. M. Huang, F. Zhao, Y. Cheng, N. Xu, and Z. Xu, ACS Nano **3**, 4062 (2009).
13. J. Bonse, J. Kruger, S. Hohm, and A. Rosenfeld, J. Laser Appl. **24**, 042006 (2012).
14. E. M. Hsu, T. H. R. Crawford, H. F. Tiedje, and H. K. Haugen, Appl. Phys. Lett. **91**, 111102 (2007).
15. Q. Wu, Y. Ma, R. Fang, Y. Liao, Q. Yu, X. Chen, and K. Wang, Appl. Phys. Lett. **82**, 1703 (2003).
16. Y. Yang, J. Yang, L. Xue, and Y. Guo, Appl. Phys. Lett. **97**, 141101 (2010).
17. J. W. Yao, C. Y. Zhang, H. Y. Liu, Q. F. Dai, L. J. Wu, S. Lan, A. V. Gopal, V. A. Trofimov, and T. M. Lysak, Opt. Express **20**, 905 (2012).
18. A. Ruiz de la Cruz, R. Lahoz, J. Siegel, G. F. de la Fuente, and J. Solis, Opt. Lett. **39**, 2491 (2014).
19. V. R. Bhardwaj, E. Simova, P. P. Rajeev, C. Hnatovsky, R. S. Taylor, D. M. Rayner, and P. B. Corkum, Phys. Rev. Lett. **96**, 057404 (2006).
20. K. U. M. Kumar and M. G. Krishna, J. Nanomater. **2008**, 1 (2008).
21. V. P. Veiko, M. V. Yarchuk, and A. I. Ivanov, Proc. SPIE **7996**, 799607 (2010).
22. B. D. Hosterman, "Raman spectroscopic study of solid solution spinel oxides," Ph.D. thesis (University of Nevada, 2011).
23. M. A. Vuurman and I. E. Wachs, J. Phys. Chem. **96**, 5008 (1992).
24. A. Vorobyev and C. Guo, Opt. Express **14**, 13113 (2006).